J Mol Model (2011) 17:2103–2111
DOI 10.1007/s00894-010-0911-5

ORIGINAL PAPER

FTIR, Raman, and UV-Vis spectroscopic and DFT investigations of the structure of iron–lead–tellurate glasses

Simona Rada · Adriana Dehelean · Eugen Culea

Received: 18 June 2010 / Accepted: 21 November 2010 / Published online: 21 December 2010

Abstract In this work, the effects of iron ion intercalations on lead–tellurate glasses were investigated via FTIR, Raman and UV-Vis spectroscopies. This homogeneous glass system has compositions $x Fe_2O_3 \cdot (100-x)[4TeO_2 \cdot PbO_2]$, where x=0–60 mol%. The presented observations in these mechanisms show that the lead ions have a pronounced affinity towards $[TeO_3]$ structural units, resulting in the deformation of the Te–O–Te linkages, and leading to the intercalation of $[PbO_n]$ (n=3, 4) and $[FeO_n]$ (n=4, 6) entities in the $[TeO_4]$ chain network. The formation of negatively charged $[FeO_4]^{1-}$ structural units implies the attraction of Pb^{2+} ions in order to compensate for this electrical charge. Upon increasing the Fe_2O_3 content to 60 mol%, the network can accommodate an excess of oxygen through the formation of $[FeO_6]$ structural units and the conversion of $[TeO_4]$ into $[TeO_3]$ structural units. For even higher Fe_2O_3 contents, Raman spectra indicate a greater degree of depolymerization of the vitreous network than FTIR spectra do. The bands due to the Pb–O bond vibrations are very strongly polarized and the $[TeO_4]$ structural units convert into $[TeO_3]$ units via an intermediate coordination stage termed "$[TeO_{3+1}]$" structural units. Our UV-Vis spectroscopic data show two mechanisms: (i) the conversion of the Fe^{3+} to Fe^{2+} at the same time as the oxidation of Pb^{2+} to Pb^{+4} ions for samples with low Fe_2O_3 contents; (ii) when the Fe_2O_3 content is high ($x \geq 50$ mol%), the Fe^{2+} ions capture positive holes and are transferred to Fe^{3+} ions through a photochemical reaction, while the Pb^{2+} ions are formed by the reduction of Pb^{4+} ions. DFT calculations show that the addition of Fe_2O_3 to lead–tellurate glasses seems to break the axial Te–O bonds, and the $[TeO_4]$ structural units are gradually transformed into $[TeO_{3+1}]$- and $[TeO_3]$-type polyhedra. Analyzing these data further indicates a gradual conversion of the lead ions from covalent to ionic environment. There is then a charge transfer between the tri- and tetracoordinated tellurium atoms due to the capacity of the lead–tellurate network to form the appropriate coordination environments containing structural units of opposite charge, such as iron ions, $[FeO_4]^{1-}$.

Keywords Iron–lead–tellurate glasses · FTIR and UV-Vis spectroscopy · DFT calculations

S. Rada (✉) · A. Dehelean · E. Culea
Department of Physics, Technical University of Cluj-Napoca,
400641 Cluj-Napoca, Romania
e-mail: Simona.Rada@phys.utcluj.ro

S. Rada
e-mail: radasimona@yahoo.com

A. Dehelean
National Institute for Research and Development of Isotopic and Molecular Technologies,
Cluj-Napoca, Romania

Introduction

Oxide glasses that include transition metal ions have been extensively studied due to their semiconducting properties [1–6]. Such conduction in ternary iron oxide glasses was found to be due to polaron hopping conduction [7].

The structural role played by lead oxide in many oxide glasses is unique, as lead oxide is known to act as both a network modifier and a network former [1, 8, 9]. The role it adopts depends on the type of bond between lead and

oxygen. Studies have proposed that it would become difficult to form the network structure of binary glass with high PbO contents [7, 8].

The structure and the properties of oxide glasses depend strongly on the nature and concentration of their constituent oxides. In a normal glass system, the modifier atoms cause the network to break. In tellurate glasses, the modifier atoms modify the basic structural units such as trigonal bipyramidal [TeO_4] and trigonal pyramidal [TeO_3], with one of the equatorial positions becoming occupied by a lone pair of electrons [9].

The objective of the work described in this paper is to analyze the structural and spectroscopic properties of iron–lead–tellurate glasses through FTIR, Raman, and UV-Vis spectroscopic investigations and DFT calculations. Particular attention is paid to attempting to understand the roles played by lead and iron ions in determining the structural properties of the glasses.

Experimental

Glasses were prepared by mixing and melting appropriate amounts of lead(IV) oxide, tellurium(IV) oxide and iron (III) oxide of high purity (99.99%, Aldrich Chemical Co.). The reagents were melted at 1000 °C at 15 min and quenched.

The samples were analyzed by means of X-ray diffraction using a XRD-6000 Shimadzu diffractometer with a graphite monochromator for Cu-Kα radiation (λ=1.54 Å) at room temperature. The X-ray diffraction patterns did not reveal a crystalline phase in samples with $x \geq 60$ mol% Fe_2O_3.

FT-IR absorption spectra of the glasses in the 370–1200 cm^{-1} spectral range were obtained with a Jasco FTIR 6200 spectrometer using the standard KBr pellet disc technique. The spectra were recorded at a standard resolution of 2 cm^{-1}.

UV-Vis absorption spectra of the powdered glass samples were recorded at room temperature in the range 250–800 cm^{-1} using a PerkinElmer Lambda 45 UV-Vis spectrometer equipped with an integrating sphere. These measurements were performed on glass powder dispersed in KBr pellets.

Raman spectra were recorded for bulk glasses using an integrated FRA 106 Raman module in a 180° scattering geometry at room temperature. The spectral resolution was 1 cm^{-1}.

Geometry optimization of the proposed structural model was carried out using density functional theory (DFT). The DFT computations were performed with the B3PW91/CEP-4 G/ECP method using the Gaussian 03 software package [10].

Results and discussion

FTIR spectroscopy

Figure 1 shows FTIR spectra of Fe_2O_3-doped lead–tellurate glasses. Examining the FTIR spectra of the $xFe_2O_3 \cdot (100-x)[4TeO_2 \cdot PbO_2]$ glasses shows that the Fe_2O_3 content modifies the characteristic IR bands as follows:

i) The larger band centered at ~625 cm^{-1} is assigned to the stretching mode of the trigonal bipyramidal [TeO_4] with bridging oxygens. The shoulder located at about 750 cm^{-1} indicates the presence of [TeO_3] structural units; see Table 1 [10–15]. For all of the glasses, the general trend is a shift towards higher wavenumbers (668 cm^{-1}) with Fe_2O_3 content. This suggests the

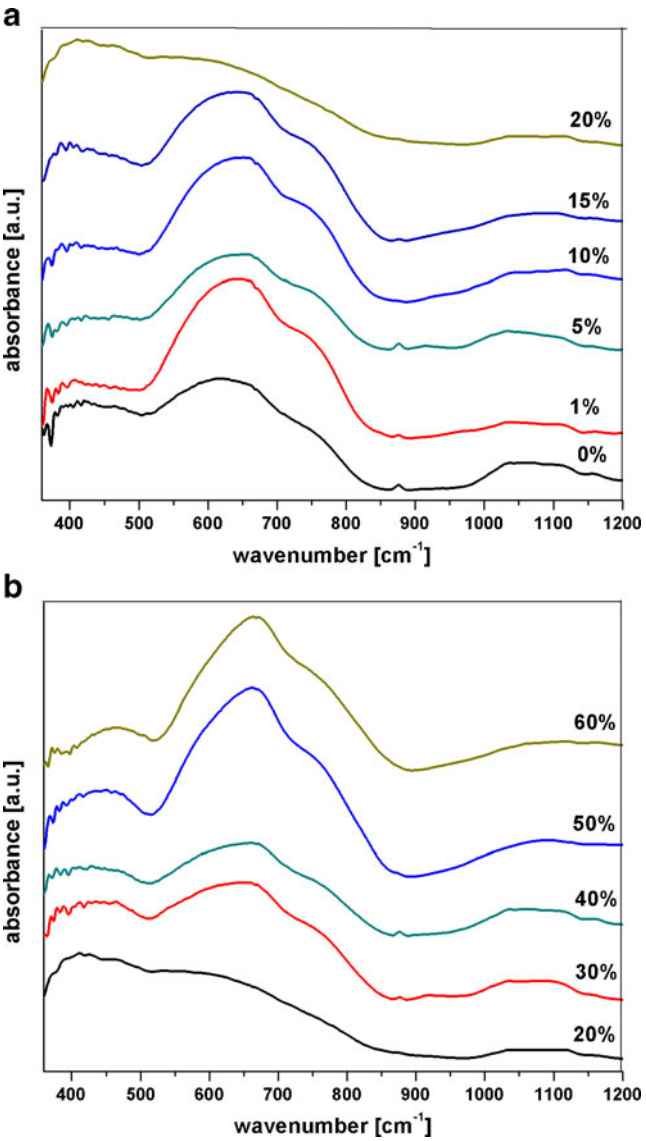

Fig. 1 FTIR spectra of $xFe_2O_3 \cdot (100-x)[4TeO_2 \cdot PbO]$ glasses with $0 \leq x \leq 60$ mol%

Table 1 Assignment of the Raman and IR bands for xFe$_2$O$_3$·(100−x)[4TeO$_2$·PbO] glasses

Raman band (cm^{-1})	IR band (cm^{-1})	Assignment
120, 135	-	Pb–O symmetric stretching vibration
270	-	Pb–O stretching and O–Pb–O bending vibrations
-	400–500	Fe–O vibrations of [FeO$_6$] structural units
405	470	Vibrations of Pb–O covalent bonds in [PbO$_4$] structural units
465	475	The stretching vibrations of Te–O–Te linkages
-	570–600	Fe–O bonds in [FeO$_4$] structural units
650–670	620–680	Stretching vibrations of [TeO$_4$] structural units
-	670, 850, 1050	Vibrations of Pb–O bonds from [PbO$_3$] and [PbO$_4$] structural units
720–735	720–780	Stretching vibrations of [TeO$_3$]/[TeO$_{3+1}$] structural units

conversion of some [TeO$_4$] to [TeO$_3$] structural units, because the lead ions have a strong affinity towards these groups containing nonbridging oxygens, which have negative charges.

ii) The broader band centered at about 670 cm^{-1} can be attributed to Pb–O bond vibrations from [PbO$_3$] and [PbO$_4$] structural units [16–19]. With increasing Fe$_2$O$_3$ content (up to 15 mol%), the formation of larger numbers of nonbridging oxygens results in the appearance of [PbO$_n$] structural units (n=3, 4) in the vicinity of the [TeO$_3$] structural units. The increase in the intensity of the band located at about 600 cm^{-1} indicates the formation of [FeO$_4$] structural units. It seems that the formation of [TeO$_4$] structural units is reduced because the modified [TeO$_3$] units containing one or more Te–O–Pb bonds are unable to accept a fourth oxygen atom.

When added to the host matrix, Fe$_2$O$_3$ (which tends to coordinate with Fe^{3+}) will coordinate with glass-forming cation ions. According to electronegativity theory, the covalency of the bond will strengthen as the difference in electronegativity between the cations and anions decreases. Since the electronegativities of Te, Fe, Pb and O are 2.1, 1.83, 2.33 and 3.5, respectively, the covalency of Pb–O is stronger than those of Te–O and Fe–O, respectively. As a result, the covalencies of the Te–O and Pb–O bonds are stronger than that of the Fe–O bond.

Accordingly, the excess nonbridging oxygen ions will coordinate with the iron ions only after the tellurium and lead cations have attained their maximum coordination numbers (four for both tellurium and lead atoms), in agreement with our FTIR data.

iii) For the sample with x=20 mol% Fe$_2$O$_3$, the action of the lead ions as network formers yields drastic modifications to the IR spectrum and a change from a lead–tellurate network to a continuous iron–lead–tellurate network that is interconnected through Pb–O–Te, Pb–O–Fe, and Te–O–Fe bridges. This compositional evolution of the structure can be explained by considering that the excess oxygen can be accommodated by the conversion of some [FeO$_4$] to [FeO$_6$] structural units. A new band appears at 470 cm^{-1} corresponding to the Fe–O vibrations from the [FeO$_6$] structural units [19].

iv) For the sample with x≥30 mol% Fe$_2$O$_3$, the tendency of the bands located in the region between 550 and 850 cm^{-1} to move towards higher wavenumbers can be explained by the conversion of [TeO$_4$] into [TeO$_3$] structural units. Thus, there is a noticeable change in the content of [TeO$_3$] structural units.

Iron in the oxidation state 3+ is reported to occur predominantly with a coordination number of four, as in [FeO$_4$]$^{1-}$. These tetrahedral ions have a negative charge and hence need cations, Pb^{2+} in the glasses studied here, for charge compensation. Accordingly, compensation of electrical charges of Pb^{2+} ions can be realized with [FeO$_4$]$^{1-}$ structural units.

These observations show that the lead ions have a pronounced affinity towards [TeO$_3$] structural units, resulting in the deformation of Te–O–Te linkages and leading to the intercalation of [PbO$_n$] (n=3, 4) and [FeO$_n$] (n=4, 6) entities into the [TeO$_4$] chain network. The formation of negatively charged [FeO$_4$]$^{1-}$ structural units implies the attraction of Pb^{2+} ions for compensation of electrical charges. By increasing of the Fe2O3 content up to 60 mol% in the matrix glass, the number of lead ions bonded ionic in the glass was increased (see the band located at about 310nm in the UV-VIS spectra).

UV-Vis spectroscopy

Iron is present in glasses as Fe^{2+} and Fe^{3+} ions, both of which can exist at tetrahedral and octahedral sites [20–25].

Each redox and coordination state produces its own set of characteristic optical absorption bands. The majority of the Fe^{3+} ions are believed to occupy tetrahedral network-forming sites in glasses, although this has been disputed [20–23]. Conversely, the majority of the Fe^{2+} ions are thought to occupy octahedral network-modifying sites [21, 24, 25].

Fe^{2+} produces an oxygen–iron charge transfer band that is centered in the ultraviolet [24]. Spin-forbidden bands are also expected at 450–550 nm, but these have been ignored in most studies of iron absorption in glasses. Fe^{2+} ions also yield two main spin-allowed *d–d* absorption bands located at about 1100 nm, which have been attributed to a range of distorted octahedral sites. Accordingly, the energy diagram of the $3d^6$ configuration (Fe^{2+}) indicates that its spectrum will essentially consist of a single band in the infrared region, as well as a number of very weak spin-forbidden bands in the visible and ultraviolet regions.

Fe^{3+} ions produce a more complicated set of absorptions than Fe^{2+}. Since the Fe^{3+} ion has a d^5 configuration, all *d–d* transitions are forbidden by spin-selection rules [26]. This means they are approximately 10–100 times less intense than spin-allowed transitions. The majority of the *d–d* bands of Fe^{3+} are observed at wavelengths in the 325–450 nm region, although some Fe^{3+} bands are observed at wavelengths as low as 700 nm.

The UV-Vis absorption spectra of $x Fe_2O_3 \cdot (100-x)[4TeO_2 \cdot PbO_2]$ glasses with x=0–60 mol% are shown in Fig. 2. An examination of these spectra shows that the characteristic UV-Vis bands are modified:

i) For all glasses, the UV absorption bands begin at 250 nm with an ascending lobe. These UV absorption bands are assumed to originate from the lead–tellurate host matrix. The stronger transitions in the UV-Vis spectrum may be due to the presence of Te=O bonds from [TeO_3] structural units and Pb=O bonds from [PbO_3] structural units, which allow n–π^* transitions. Pb^{2+} ions with the s^2 configuration absorb strongly in the ultraviolet and yield broad emission bands in the ultraviolet and blue spectral regions. The intense band centered at about 310 nm corresponds to these Pb^{2+} ions [27].

ii) Upon introducing a low content of Fe_2O_3 ($x \leq 5$ mol%) into the host matrix, new UV absorption bands appear. These bands, located in the 320–450 nm region, are due to the presence of the Fe^{3+} ions. The intensity of the absorption band located at about 250 nm increases, and the iron in some cases is reduced to Fe^{2+} through electron trapping [28]. Some weak bands appear in the 450–550 nm region. These bands show that some Fe^{3+} ions were converted to Fe^{2+} ions.

Such a tendency can be interpreted by invoking the conversion of Fe^{3+} to Fe^{2+} at the same time as Pb^{2+} ions are oxidized to Pb^{4+} ions. Based on these experimental results, we propose the following possible redox reactions:

$$2Fe^{3+} + 2e^- \leftrightarrow 2Fe^{2+}$$

$$Pb^{2+} \leftrightarrow Pb^{4+} + 2e^-$$

The increased intensity of the band situated near 300 nm can be attributed to the formation of new Pb=O bonds from [PbO_3] structural units.

iii) Adding Fe_2O_3 content until it reaches 15 mol% causes a decrease in the intensities of the UV absorption bands situated in the 320–450 nm domain. This

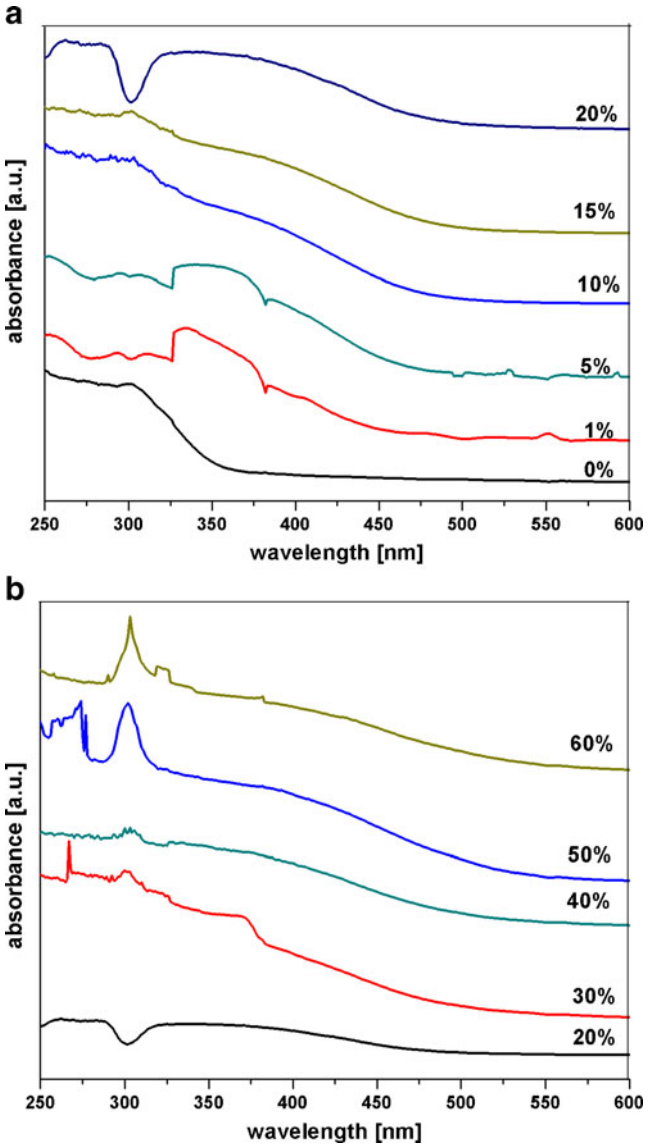

Fig. 2 UV-Vis absorption spectra of $x Fe_2O_3 \cdot (100\text{-}x)[4TeO_2 \cdot PbO]$ glasses as a function of iron oxide content

noticeable decrease could be due to iron ions acting as network formers. The sharp increases in the intensities of the IR bands located at about 600 cm^{-1} result from the vibrations of Fe–O bonds in [FeO_4] tetrahedral structural units (Fig. 1).

iv) Upon further increasing the content of Fe_2O_3 up to 20 mol%, a shift in the UV band from 250 to 260 nm is observed, and a new band located at about 285 nm appears, which are correlated with the possible distortion of the symmetry of the iron species. The new IR band situated at about 470 cm^{-1} can be attributed to octahedral [FeO_6] units. The evolution of the structure can be explained by considering that the network accommodates excess oxygen by converting some [FeO_4] to [FeO_6] structural units.

v) For the sample with x=30 mol% Fe_2O_3, a new band appears at about 267 nm. This can again be explained by distortions of the iron species. It is possible that [FeO_6] is converted to [FeO_4] structural units. The intensity of the band centered at about 600 cm^{-1} increases in the FTIR spectrum. These geometric interconversions decrease as the Fe_2O_3 content increases up to 40 mol%.

vi) Very intense transitions appear in the sample with x= 50 mol% Fe_2O_3. A new highly intense band situated at about 305 nm is due to the presence of Pb^{2+} ions. The bands located in the 250–277 nm region are due to strong oxygen–iron charge transfer associated with the Fe^{2+} and Fe^{3+} ions. The increase in the intensity of the IR band located at about 689 cm^{-1} relates to the vibrations of Fe^{2+}–O–Fe^{3+} linkages [19]. On the other hand, these intense transitions could be due to the formation of [TeO_3] structural units from [TeO_{3+1}] structural units, in agreement with the Raman spectra.

vii) For the sample with x=60 mol% Fe_2O_3, the UV absorption bands situated in the 250–290 nm region disappear and new bands appear at 320 nm. These bands show the presence of new Fe^{3+} ions. The kink located at about 430 nm is characteristic of Fe^{3+} ions with octahedral symmetry. Also, it is proposed that some of the Fe^{2+} ions capture positive holes and are converted to Fe^{3+} according to the following photochemical reactions:

$$Fe^{2+} + \text{positive holes} \rightarrow Fe^{3+}$$

$$Pb^{4+} + 2e^{-} \rightarrow Pb^{2+}$$

It seems that some of the Fe^{2+} ions capture positive holes and are converted to Fe^{3+} ions through a photochemical reaction. This mechanism explains the observed increase in the UV region.

The observed continuous increase in UV band intensity upon the addition of Fe_2O_3 can be related to the progressive growth in induced color centers. These color centers are obviously correlated with the transformation of Fe^{2+} to Fe^{3+} ions through the capture of positive holes.

In brief, the UV-Vis spectroscopic data show two mechanisms: (i) the conversion of Fe^{3+} to Fe^{2+} at the same time as the oxidation of Pb^{2+} to Pb^{4+} ions in samples with low Fe_2O_3 contents; (ii) when the Fe_2O_3 content is relatively high ($x \geq 50$ mol%), the Fe^{2+} ions capture positive holes and are converted into Fe^{3+} ions in a photochemical reaction, while the Pb^{2+} ions are formed by the reduction of Pb^{4+} ions.

The conduction of ternary iron oxide glasses was found to be due to polaron hopping conduction [1, 4–7]. In the conduction mechanism of these glasses, a valence change, $Fe^{2+} \rightarrow Fe^{3+} + e^{-}$, takes place in the glass. The Fe^{3+} ions in excess have a coordination number of six and the remaining Fe^{3+} ions have a coordination number of four. Redox can also control the tetrahedral to octahedral Fe^{3+} ratio: increasing Fe^{3+} leads to an increase in octahedral Fe^{3+}.

DFT calculations

We will use the IR and UV-Vis data in the quantum chemical calculations in order to gain a better understanding of the local structure $50Fe_2O_3 \cdot 50[4TeO_2 \cdot PbO_2]$. A similar methodology was previously used to study other glasses [29–33]. The local structure of the proposed model for matrix network were found by optimization (Fig. 3).

There are some sites in our model (Fig. 3), namely:

i) The basic coordination polyhedrons are [TeO_4] structural units, which can be found in the glass in four states: tetrahedral, square pyramidal, trigonal bipyramidal, and trigonal bipyramidal with three strong bonds and one elongated axial bond. The Te–O bonds from the square pyramids have shorter interatomic distances (2×1.74 and 2×1.85 Å) than the covalent Te–O bond length (2.15 Å). The Te–O bonds from the tetrahedral geometry have one bond with a shorter interatomic distance (1.78 Å) and three bonds with longer interatomic distances (1.87 Å).

The Te–O bonds of the irregular polyhedrons are subdivided into two groups: (1) three bonds have shorter interatomic distances (1.74–1.82 Å) and one with an intermediate interatomic distance (1.92–2.02 Å); (2) three bonds with intermediate interatomic distances (1.95–2.05 Å) and one with a longer interatomic distance (3.05 Å), but this is still significantly shorter than the sum of the van der Waals radii (3.58 Å). These irregular polyhedrons are situated in the vicinity of the [PbO_n] and [FeO_n] structural units.

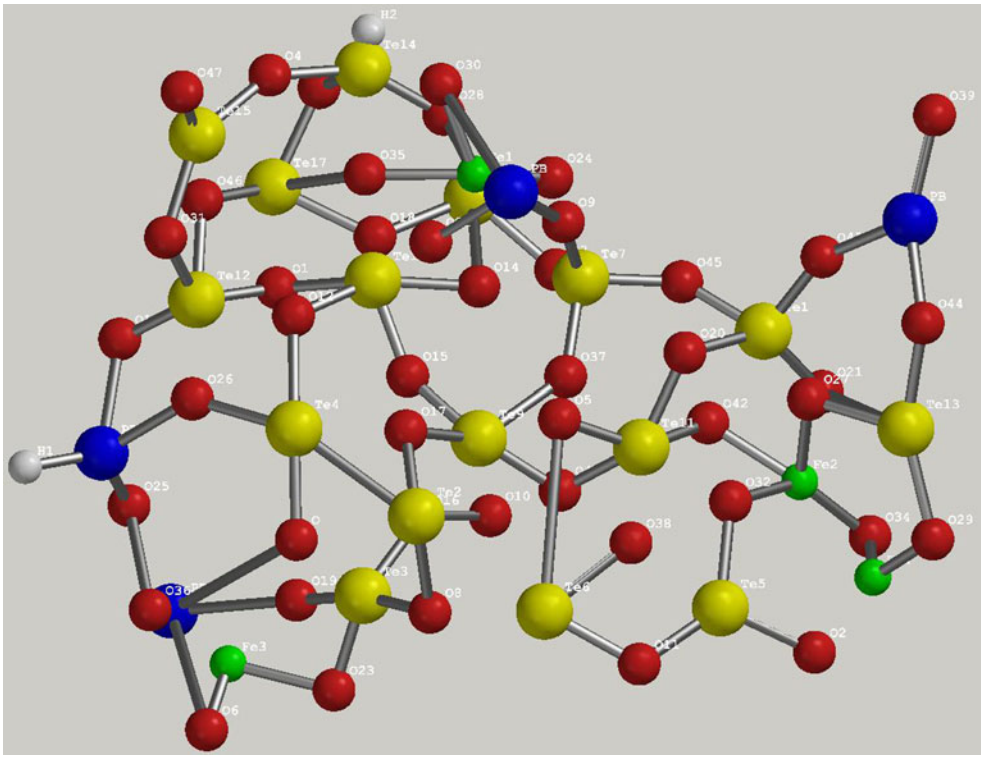

Fig. 3 The optimized structure of the $50Fe_2O_3{\cdot}50[4TeO_2{\cdot}PbO]$ glass was used to perform the DFT computations

Accordingly, the $[TeO_4]$ structural units show a marked tendency to deform, as well as enhanced lability of one of the axial bonds. This lability is sharply increased in the liquid state, where due to kinetic factors the axial bonds easily undergo dynamic elongation to over 2.15 Å. The coordination number of the tellurium atom changes from four to (3+1), and a marked tendency for elongation of the Te–O distance to over 2.15 Å is observed. As a consequence, (3+1) coordination of the tellurium is required. Besides the kinetic factors, the extent of bond deformation is also influenced by the composition, temperature and viscosity of the melt, the nature of the modifier, and by some thermodynamic factors.

ii) The presence of $[TeO_3]$ polyhedra in the glass is also possible, and depends strongly on the modifier concentration. The Te–O distances are divided into three sets: a set of three shorter distances ranging from 1.79 to 1.85 Å; three intermediate bonds ranging from 1.93 to 2.06 Å, and one longer interatomic distance (3.39 Å).

iii) In this structure, four-coordinated lead atoms occupy two different sites. At the first site they are coordinated with four oxygen atoms, thus leading to distorted tetrahedral octahedral geometries where the four Pb–O bonds have short interatomic distances (1.98–2.13 Å). The lead atoms at the second site have ionic character. One Pb–O bond has a shorter interatomic distance (2.11 Å) and one has a longer Pb–O bond distance (2.83 Å) than the Pb–O covalent bond (2.22 Å), but both are still significantly shorter than the sum of the van der Waals radii (3.54 Å), and the two oxygen atoms remain relatively far from the lead cation (4.12–4.75 Å). These bonds are too long to be chemical bonds in the usual sense.

iv) The three-coordinated lead atoms occur at two different sites. At the first site, the three bonds have short interatomic distances (1.90–2.06 Å). At the other site, two bonds have short interatomic distances (2.19–2.21 Å) and one Pb–O bond has a long interatomic distance (2.96 Å) than the Pb–O covalent bond.

v) Iron is coordinated to four oxygen atoms. Three of these bonds have short Fe–O interatomic distances (1.79–1.87 Å) while one has a long interatomic distance (1.93 Å). EXAFS analysis [34] reveals that in the iron glasses, the Fe–O bond length in the $[FeO_4]$ tetrahedral structural units is equal to 1.86–1.88 Å. The distance of 1.93 Å is intermediate between that corresponding to tetrahedrally (1.88 Å) and octahedrally (2.00 Å) coordinated iron [35]. Therefore, in this sample, it is expected that the iron atoms occupy both tetrahedral and octahedral sites. The majority of the Fe^{3+} ions are believed to occupy tetrahedral network-forming sites in glasses, while the majority of the Fe^{2+} ions are thought to occupy octahedral network-modifying sites. If in the during melting of glass Fe^{+3} ions were undergo to process of reduction at Fe^{+2} ions, ionii Fe^{+2} will cause the formation of $[FeO_6]$ structural units.

Additionally, the EXAFS analysis [34] disclosed that the coordination number of the iron depends on the Fe_2O_3 concentration. Accordingly, the number of oxygen atoms in the $[FeO_4]$ structural units decreases when the Fe_2O_3 concentration increases, suggesting that the tetrahedral coordination of iron in the glass is destroyed.

The distributions of the electronic states in the HOMO and the LUMO can be seen in Fig. 4. Interesting findings for these systems include the following:

i) The HOMO gives the $[TeO_4]$ structural units electron-donating character.
ii) The LUMO gives the $[TeO_3]$ structural units of the network electron-accepting character.
iii) The $HOMO^{-1}$ gives the $[TeO_4]$ and $[TeO_3]$ structural units and the Fe^{2+} ions electron-donating character.
iv) The $LUMO^{+1}$ gives the $[TeO_3]$ and $[TeO_4]$ structural units of the network electron-accepting character.

There is change transfer between the tri- and tetracoordinated tellurium atoms. This can be explained by noting that the lead–tellurate network is sufficiently flexible to form the appropriate coordination environment for structural units of opposite charge, such as the iron ions $[FeO_4]^{1-}$.

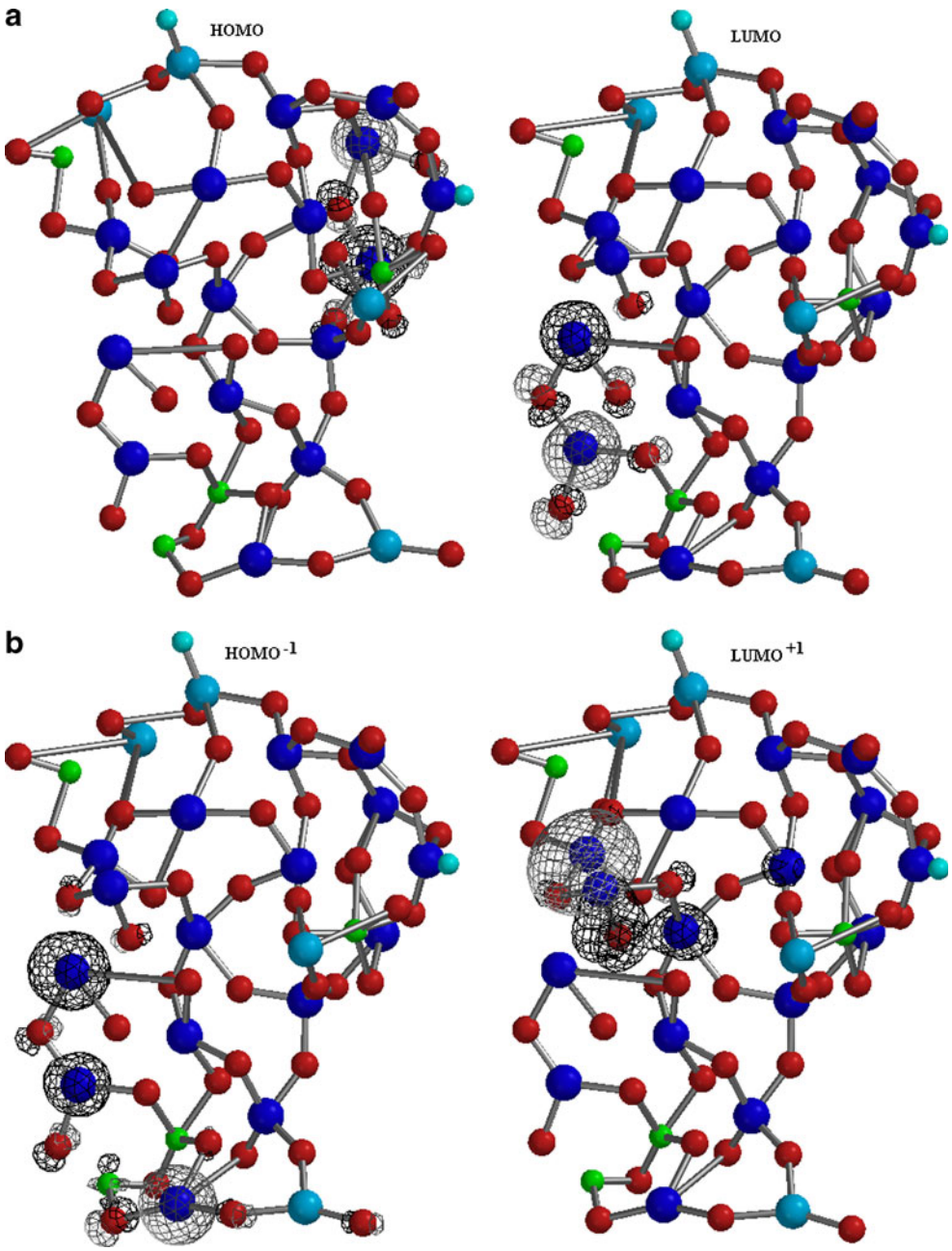

Fig. 4 Distributions of the electronic states for the HOMO (E_{HOMO}=−6.03 eV), $HOMO^{-1}$, LUMO (E_{LUMO} = −1.73 eV) and $LUMO^{+1}$ of the proposed model for $50Fe_2O_3{\cdot}50[4TeO_2{\cdot}PbO]$ glasses

Accordingly, the addition of Fe_2O_3 content to lead–tellurate glasses appears to break the axial Te–O bonds because of the strong polarizability of the lone pair electrons on tellurium, leading to the formation of the glass structure. As a result, more nonbridging Te–O bonds are formed and the [TeO_4] structural units are gradually transformed into [TeO_{3+1}]- and [TeO_3]-type polyhedra as the metal oxides are slowly added. The analysis of these data further indicates that increasing the concentration of Fe_2O_3 leads to a gradual conversion of lead ions from covalent to ionic environment.

Raman spectroscopy

Figure 5 shows the Raman spectra of the $x$$Fe_2O_3$·(100−$x$)[4$TeO_2$·$PbO_2$] glasses with x=0–60 mol%. The shape of the Raman spectrum is influenced by the presence of iron oxide in the studied glass. The bands centered at around 465 cm^{-1} are assigned to the stretching vibrations of Te–O–Te linkages [36]. The bands centered at around 652 cm^{-1} originate from vibrations of the continuous tetragonal bipyramidal [TeO_4] network, and the bands centered at around 710 cm^{-1} are from the [TeO_{3+1}] and [TeO_3] structural units [37]. It was found that the maximum phonon energy of the doped glasses gradually increased from 710 to 745 cm^{-1}. As the Fe_2O_3 content increases up to 60 mol%, the numbers of polyhedral [TeO_{3+1}] and trigonal pyramidal [TeO_3] structural units increase in the network structure.

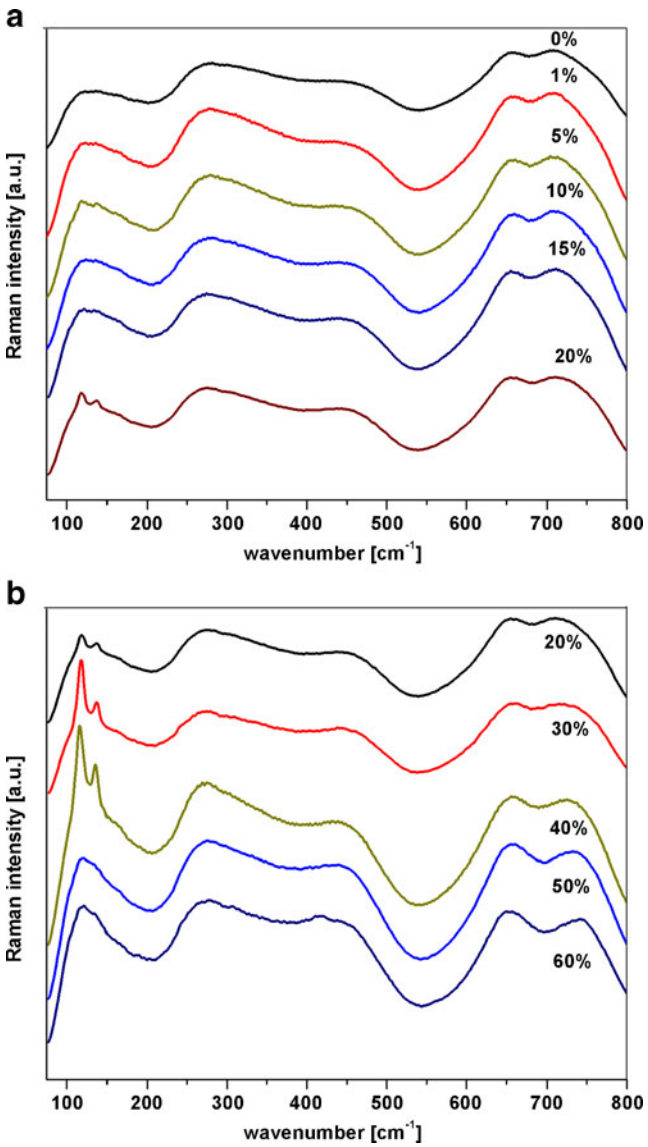

Fig. 5 Raman spectra of $x$$Fe_2O_3$·(100−$x$)[4$TeO_2$·PbO] glasses with 0≤$x$≤60 mol%

The [TeO_{3+1}] unit can be thought of as a distorted trigonal bipyramidal [TeO_4] unit with one oxygen further from the central tellurium than the remaining three oxygens. This increase in units with lower coordination numbers at the expense of units with higher coordination numbers is indicative of the depolymerization of the lead–tellurite glass network.

The Raman band centered at about 270 cm^{-1} may be associated with Pb–O stretching and O–Pb–O bending vibrations. The strong bands situated near 120 and 135 cm^{-1} in the Raman spectra of iron–lead–tellurate glasses are almost certainly due to Pb–O symmetric stretching vibrations [38, 39]. Support for this comes from the fact that the relative intensity of this band increases with increasing Fe_2O_3 content of the glass from x=1 to 40 mol % Fe_2O_3, but the intensity decreases markedly for higher Fe_2O_3 contents than this. This shows that a high Fe_2O_3 content can lead to broken Pb–O bonds in iron–lead–tellurate glasses. On the other hand, this is necessary because the content of [TeO_3] structural units increases. For samples with x≥50 mol%Fe_2O_3, the increased intensities of the UV-Vis bands located at about 310 nm support this hypothesis.

The fact that this band is very strongly polarized also indicates that the nearest neighbors of lead atoms have a high degree of symmetry [38]. While there is a drop in the intensity of the band at 135 cm^{-1}, no new bands appear in the Raman spectra. By increasing of Fe_2O_3 content up to 40 mol%, the intensity of the band situated at about 135 cm-1 attains its maximum value. We think that a higher doping level can result in broken Pb–O bonds and cause the [PbO_4] structural units to change to [PbO_3] chains [40]. For the sample with x=60 mol%, a supplementary, well-defined Raman band appears at around 415 cm^{-1}. This band is due to covalent Pb–O bond vibrations [41, 42].

For higher Fe_2O_3 contents, the Raman spectra indicate a greater degree of depolymerization of the vitreous network than the FTIR spectra do. It thus appears that Raman spectroscopy is a more sensitive technique to the changes that appear in the short-range order of the structure of our glass upon Fe_2O_3 addition.

Conclusions

We analyzed the effects of iron ions on the structure of lead–tellurate glasses using FTIR, Raman, and UV-Vis spectroscopies. Based our results, we can conclude that the network can accommodate excess oxygen by deforming Te–O–Te linkages, the actions of lead and iron atoms as network formers, and the intercalation of [FeO_6] entities into the [TeO_4] chain network.

Our UV-Vis spectroscopic data show the occurrence of a reversible redox process in the matrix host upon increasing the Fe_2O_3 content. For small Fe_2O_3 contents, the mechanism implies the conversion of Fe^{3+} to Fe^{2+} at the same time as the oxidation of Pb^{2+} to Pb^{4+}. Inverted redox processes take place at higher Fe_2O_3 contents.

DFT calculations show that the [TeO_4] structural units show a marked tendency to deform and for enhanced lability of one of the axial bonds. This can be explained by noting that that the lead–tellurate network is sufficiently flexible to form the appropriate coordination environment for structural units with opposite charges such as the iron ions $[FeO_4]^{-1}$.

The Raman spectra show that very strong depolymerization appears in studied iron–lead–tellurate glasses with the addition of Fe_2O_3. The bands due to the Pb–O bond vibrations are very strongly polarized, indicating that the nearest neighbors of lead atoms have a high degree of symmetry. The intensity of the band around 720 cm^{-1} increases relative to the band at 660 cm^{-1} with increasing Fe_2O_3 content, indicating that the [TeO_4] structural units convert into [TeO_3] units via an intermediate coordination stage, termed [TeO_{3+1}] structural units.

Acknowledgments The financial support of the Ministry of Education and Research of Romania—National University Research Council (CNCSIS, PN II-IDEI 183/2008, contract number 476/2009) is gratefully acknowledged by the authors.

References

1. Dhawan VK, Mansingh A, Sayer M (1982) J Non-Cryst Solids 51:87–103
2. Sega K, Kasai H, Sakata H (1998) Mater Chem Phys 53:28–33
3. Qiu HH, Ito T, Sakata H (1999) Mater Chem Phys 58:243–248
4. Qiu HH, Kudo M, Sakata H (1997) Mater Chem Phys 51:233–238
5. Simon S, Pop R, Simon V, Coldea M (2003) J Non-Cryst Solids 331:1–10
6. Simon S, Todea M (2006) J Non-Cryst Solids 352:2947–2951
7. Pan A, Ghosh A (2002) J Mater Sci Lett 21:395–396
8. Pisarski W, Goryczka T, Wodecka-Dus B, Plonska M, Pisarska J (2005) Mater Sci Eng B 122:94–99
9. Hoppe U, Yousef E, Rüssel C, Neuefeind J, Hannon AC (2002) Solid State Commun 123:273–278
10. Frisch MJ, Trucks GW, Schlegel HB, Scuseria GE, Robb MA, Cheeseman JR, Montgomery JA Jr, Vreven T, Kudin KN, Burant JC, Millam JM, Iyengar SS, Tomasi J, Barone V, Mennucci B, Cossi M, Scalmani G, Rega N, Petersson GA, Nakatsuji H, Hada M, Ehara M, Toyota K, Fukuda R, Hasegawa J, Ishida M, Nakajima T, Honda Y, Kitao O, Nakai H, Klene M, Li X, Knox JE, Hratchian HP, Cross JB, Adamo C, Jaramillo J, Gomperts R, Stratmann RE, Yazyev O, Austin AJ, Cammi R, Pomelli C, Ochterski JW, Ayala PY, Morokuma K, Voth GA, Salvador P, Dannenberg JJ, Zakrzewski VG, Dapprich S, Daniels AD, Strain MC, Farkas O, Malick DK, Rabuck AD, Raghavachari K, Foresman JB, Ortiz JV, Cui Q, Baboul AG, Clifford S, Cioslowski J, Stefanov BB, Liu G, Liashenko A, Piskorz P, Komaromi I, Martin RL, Fox DJ, Keith T, Al-Laham MA, Peng CY, Nanayakkara A, Challacombe M, Gill PMW, Johnson B, Chen W, Wong MW, Gonzalez C, Pople JA (2003) Gaussian 03, revision A1. Gaussian Inc., Pittsburgh
11. Rada S, Culea M, Culea (2008) J Non-Cryst Solids 354:5491–5495
12. Rada S, Rada M, Culea E (2010) Spectrochim Acta A 75:846–851
13. Rada S, Culea M, Rada M, Culea E (2010) J Alloys Compd 490:270–276
14. Rada S, Neumann M, Culea E (2010) Solid State Ionics 181:1164–1169
15. Mandal S, Hazra S, Ghosh A (1994) J Mater Sci Lett 13:1054–1055
16. Hazra S, Ghosh A (1995) J Mater Res 10:2374–2378
17. Rada S, Culea M, Neumann M, Culea E (2008) Chem Phys Lett 460:196–199
18. Rada S, Ristoiu T, Rada M, Coroiu I, Maties V, Culea E (2010) Mater Res Bull 45:69–73
19. Zhang Z (1993) Phys Chem Glasses 34:95–103
20. Carnevale A, Peterson GE, Kurkjian CR (1976) J Non-Cryst Solids 22:269–275
21. Montenero A, Friggeri M, Giori DC, Belkhiria N, Pye LD (1986) J Non-Cryst Solids 84:45–60
22. Kurkjian CR (1970) J Non-Cryst Solids 3:157–194
23. Park JW, Chen H (1980) J Non-Cryst Solids 40:515–525
24. Edwards RJ, Paul A, Douglas RW (1972) Phys Chem Glasses 13:137–143
25. Rossano S, Ramos A, Delaye JM, Filipponi A, Creux S, Brouder C, Calas G (1999) J Synchrotron Radiat 6:247–248
26. Burns RG (1993) Mineralogical applications of crystal field theory. Cambridge University, Cambridge, p 57
27. Ehrt D (2004) J Non-Cryst Solids 34:822–829
28. Friebele EJ (1991) In: Ullmann DR, Kreidl NJ (eds) Optical properties of glass. American Ceramic Society, Westerville, p 205
29. Rada S, Chelcea R, Culea M, Dehelean A, Culea E (2010) J Mol Struct 977:170–174
30. Rada S, Culea M, Culea E (2008) J Phys Chem A 112:11251–11255
31. Rada S, Culea E (2009) J Mol Struct 929:141–148
32. Rada S, Culea E, Neumann M (2010) J Mol Model 16:1333–1338
33. Rada S, Chelcea R, Culea E (2010) J Mol Model. doi:101007/s00894-010-0706-8
34. Pinakidou F, Katsikini M, Kavouras P, Komninou F, Karakostas T, Paloura EC (2008) J Non-Cryst Solids 354:105–111
35. Lynn JW, Erwin RW, Rhyne JJ, Chen HS (1983) J Magn Magn Mater 31–34:1397–1398
36. Salem SM (2010) J Alloys Compd 503:242–247
37. Upender G, Sathe VG, Mouli VC (2010) Phys B 405:1269–1273
38. Jia H, Chen G, Wang W (2006) Opt Mater 29:445–448
39. Barney ER, Hannon AC, Holland D, Winslow D, Rijal B, Affatigato M, Feller SA (2007) J Non-Cryst Solids 353:1741–1747
40. Imaoka M, Hasegawa H, Yasui I (1986) J Non-Cryst Solids 85:393–412
41. Ciceo-Lucacel R, Marcus C, Timar V, Ardelean I (2007) Solid State Sci 9:850–854
42. Radu A, Baia L, Kiefer W, Simon S (2005) Vib Spectrosc 39:127–130